Impurity transport in temperature gradient driven turbulence

A. Skyman, H. Nordman, and P. Strand

Citation: Phys. Plasmas **19**, 032313 (2012); doi: 10.1063/1.3695014
View online: http://dx.doi.org/10.1063/1.3695014
View Table of Contents: http://pop.aip.org/resource/1/PHPAEN/v19/i3
Published by the American Institute of Physics.

Impurity transport in temperature gradient driven turbulence

A. Skyman,[a] H. Nordman,[b] and P. Strand[c]
Euratom–VR Association, Department of Earth and Space Sciences, Chalmers University of Technology, SE-412 96 Göteborg, Sweden, URL: http://www.chalmers.se/rss/EN/research/research-groups/transport-theory/

(Received 5 July 2011; accepted 20 February 2012; published online 28 March 2012)

In the present paper, the transport of impurities driven by trapped electron (TE) mode turbulence is studied. Non-linear (NL) gyrokinetic simulations using the code GENE are compared with results from quasilinear (QL) gyrokinetic simulations and a computationally efficient fluid model. The main focus is on model comparisons for electron temperature gradient driven turbulence regarding the sign of the convective impurity velocity (pinch) and the impurity density gradient R/L_{n_Z} (peaking factor) for zero impurity flux. In particular, the scaling of the impurity peaking factors with impurity charge Z and with driving temperature gradient is investigated and compared with results for the more studied ion temperature gradient (ITG) driven turbulence. The question of helium ash removal in TE mode turbulence is also investigated. In addition, the impurity peaking is compared to the main ion peaking obtained by a self-consistent fluid calculation of the density gradients corresponding to zero particle fluxes. For the scaling of the peaking factor with impurity charge Z, a weak dependence is obtained from NL GENE and fluid simulations. The QL GENE results show a stronger dependence for low Z impurities and overestimates the peaking factor by up to a factor of two in this region. As in the case of ITG dominated turbulence, the peaking factors saturate as Z increases, at a level much below neoclassical predictions. The scaling with Z is, however, weak or reversed as compared to the ITG case. The results indicate that TE mode turbulence is as efficient as ITG turbulence at removing He ash, with $D_{He}/\chi_{eff} > 1.0$. The scaling of impurity peaking with the background temperature gradients is found to be weak in the NL GENE and fluid simulations. The QL results are also here found to significantly overestimate the peaking factor for low Z values. For the parameters considered, the background density gradient for zero particle flux is found to be slightly larger than the corresponding impurity zero flux gradient. [http://dx.doi.org/10.1063/1.3695014]

I. INTRODUCTION

The transport properties of impurities is of high relevance for the performance and optimisation of magnetic fusion devices. For instance, the possible accumulation of He ash in the core of the reactor plasma will serve to dilute the fuel, thus lowering fusion power. Heavier impurity species, originating from the plasma-facing surfaces, may also accumulate in the core, and wall-impurities of relatively low density may lead to unacceptable energy losses in the form of radiation.[1] In an operational power plant, both impurities of low and high charge numbers will be present.

In the confinement zone of tokamaks, the transport of the background species is usually dominated by turbulence. The trapped electron (TE) mode and the ion temperature gradient (ITG)[2] mode are expected to be the main contributors. Turbulent impurity transport has been investigated in a number of theoretical[3–23] and experimental[24–28] papers. In tokamak experiments, also the impurity transport is usually dominated by turbulence, resulting in impurity peaking factors well below the neoclassical predictions.[18–23,28,29] The main theoretical effort has, with a few exceptions,[5,10,21,30] hitherto been devoted to quasilinear studies, primarily focused on ITG mode driven impurity transport. For the directly reactor relevant regimes, however, where α-particle heating dominates, as will be the case in the ITER device, or in electron cyclotron resonance heated plasmas, TE mode driven impurity transport will likely be important.

In the present study, transport of impurities driven by TE mode turbulence is investigated by non-linear (NL) gyrokinetic simulations using the code GENE.[31–33] The simulation results are compared to quasilinear (QL) gyrokinetic simulations as well as results obtained from a multi-fluid model.[34] The fluid model is employed for the dual purposes of benchmarking a computationally efficient model, suitable for predictive simulations, and interpreting the results. The TE mode results are compared with the more well known results for ITG mode dominated turbulence, obtained from QL gyrokinetic and fluid simulations.

The impurity diffusivity (D_Z) and convective velocity (V_Z) are estimated from simulation data, and from these the zero-flux impurity density gradient ($R/L_{n_Z} = -RV_Z/D_Z$), also referred to as the impurity peaking factor (PF), is derived. This quantity expresses the impurity density gradient at which the convective and diffusive transport of impurities are exactly balanced. The sign of PF is of special interest, as it determines whether the impurities are subject

[a]Electronic mail: andreas.skyman@chalmers.se.
[b]Electronic mail: hans.nordman@chalmers.se.
[c]Electronic mail: par.strand@chalmers.se.

to an inward ($PF > 0$) or outward ($PF < 0$) pinch. Scalings of peaking factors with impurity charge (Z), electron and ion temperature gradients ($\nabla T_{e,i}$), and electron density gradient (∇n_e) are studied, giving particular attention to ∇T_e driven TE mode impurity transport. The important question of how efficient the removal of helium ash will be is also investigated for TE mode turbulence using NL GENE and fluid simulations. The results are compared and contrasted with results from previous studies focused on ITG driven impurity transport. In addition, the impurity peaking relative to the main ion peaking in the plasma core obtained from a self-consistent treatment of the particle fluxes will be discussed. This situation is experimentally relevant in situations with edge particle fuelling where the steady state gradient corresponds to zero particle flux.

The remainder of the paper is structured as follows: first the transport models are reviewed, beginning with of the fluid model employed (Sec. II A) where the focus is on the impurity dynamics. This is followed by a brief introduction of the gyrokinetic model and the GENE code (Sec. II B) and a section on the specifics of the simulations (Sec. III). After this, the main results are covered, including discussion and interpretation of the acquired results (Sec. IV). The final section of the paper is a summary of the main conclusions to be drawn (Sec. V).

II. TRANSPORT MODELS

A. Fluid theory

The Weiland multi-fluid model[34] consists of coupled sets of equations for each constituent particle species: main ions, electrons, and impurities.[3,17,20,23,35] Effects of toroidal rotation are not included here. Neglecting finite Larmor radius effects, the impurity equations of continuity, parallel motion, and energy take the form of Eqs. (1a)–(1c)

$$(\widetilde{\omega}+\tau_Z^*)\widetilde{n}_Z-\left(\frac{R}{2L_{n_Z}}-\lambda\right)\widetilde{\phi}+\tau_Z^*\widetilde{T}_Z-\frac{k_\parallel\delta v_{\parallel Z}}{\omega_{D_e}}=0, \quad (1a)$$

$$(\widetilde{\omega}-2\tau_Z^*)\frac{k_\parallel\delta v_{\parallel Z}}{\omega_{D_e}}=\frac{Z}{A_Z q_*^2}\widetilde{\phi}+\frac{\tau_Z}{A_Z q_*^2}(\widetilde{n}_Z+\widetilde{T}_Z), \quad (1b)$$

$$\left(\widetilde{\omega}+\frac{5}{3}\tau_Z^*\right)\widetilde{T}_Z-\left(\frac{R}{2L_{T_Z}}-\frac{1}{3}\frac{R}{L_{n_Z}}\right)\widetilde{\phi}-\frac{2}{3}\widetilde{\omega}\widetilde{n}_Z=0. \quad (1c)$$

In Eqs. (1a)–(1c), $\widetilde{n}_Z=\delta n_z/n_Z$ is the density, $\widetilde{\phi}=e\phi/T_e$ is the electrostatic potential, $\widetilde{T}_Z=\delta T_Z/T_Z$ is the temperature, and $\delta v_{\parallel Z}$ is the parallel velocity. The normalised eigenvalue and wave vector of the eigenmodes are $\widetilde{\omega}=\widetilde{\omega}_r+\mathrm{i}\gamma$ and $\boldsymbol{k}=k_\parallel\hat{z}+\boldsymbol{k}_\perp$, $\sim$ denoting normalisation with respect to the electron magnetic drift frequency ω_{De}. The normalised scale lengths can be assumed to be constant for the flux tube domain considered and are defined as $\frac{R}{L_{X_j}}=-\frac{R}{X_j}\frac{\partial X_j}{\partial r}$, where R is the major radius of the tokamak, and $X_j=n_j,T_j$ for species j. The other parameters are defined as follows: $\tau_Z^*=\lambda T_Z/ZT_e$ with $\lambda=\cos\theta+s\theta\sin\theta$ for the poloidal angle $\theta,\tau_Z=T_Z/T_e,A_Z=m_Z/m_i\approx 2Z$ is the impurity mass number, and Z is the impurity charge. Further, s is the magnetic shear and $q^*=2qk_\theta\rho_s$, where q is the safety factor, $\rho_s=c_s/\Omega_{ci}$ is the ion sound scale with the ion sound speed $c_s=\sqrt{T_e/m_i}$, and the ion cyclotron frequency $\Omega_{ci}=eB/m_i$. Effects of curvature enter the equations through the magnetic drift, defined as $\omega_{D_Z}=\omega_{D_Z}^{\theta=0}\lambda(\theta)$, which originates from the compression of the $\boldsymbol{E}\times\boldsymbol{B}$ drift velocity, the diamagnetic drift velocity, and the diamagnetic heat flow. Curvature effects from the stress tensor enter as $2\tau_Z^*$ at the left hand side of Eq. (1b).

Combining Eqs. (1a)–(1c), while neglecting pressure perturbations in Eq. (1b) for simplicity, the relation of the electrostatic potential $\widetilde{\phi}$ and impurity density $\widetilde{n}_Z$ becomes

$$\widetilde{n}_Z=\left[\widetilde{\omega}\left(\frac{R}{2L_{n_Z}}-\lambda\right)-\tau_Z^*\left(\frac{R}{2L_{T_Z}}-\frac{7}{3}\frac{R}{2L_{n_Z}}+\frac{5\lambda}{3}\right)+\frac{Z}{A_Z q_*^2}\left(\frac{\widetilde{\omega}+5\tau_Z^*/3}{\widetilde{\omega}-2\tau_Z^*}\right)\right]\frac{\widetilde{\phi}}{N}, \quad (2)$$

where

$$N=\widetilde{\omega}^2+\frac{10\tau_Z^*}{3}\widetilde{\omega}+\frac{5\tau_Z^{*2}}{3}. \quad (3)$$

The main ion and electron response is calculated from the corresponding fluid equations for ions and trapped electrons. The electron response is given by a trapped and a free part such that $\frac{\delta n_e}{n_e}=f_t\frac{\delta n_{e_t}}{n_{e_t}}+(1-f_t)\frac{e\phi}{T_e}$, i.e., the free electrons are assumed to be adiabatic and thus to follow the Boltzmann distribution $\delta n_{e_f}/n_{e_f}=e\phi/T_e$.

The equations are closed by the assumption of quasi-neutrality

$$\frac{\delta n_e}{n_e}=(1-Zf_Z)\frac{\delta n_i}{n_i}+Zf_Z\frac{\delta n_Z}{n_Z}, \quad (4)$$

where $f_Z=\frac{n_Z}{n_e}$ is the fraction of impurities.

Thus, an eigenvalue equation for TE and ITG modes is obtained in the presence of impurities. Assuming a strongly ballooning eigenfunction with[36] $k_\parallel^2=(3q^2R^2)^{-1}$, the eigenvalue equation is reduced to a system of algebraic equations that is solved numerically. The sensitivity of the fluid results to the choice of $k_\parallel$ will be examined in Sec. IV A.

The zero-flux impurity peaking factor, defined as $PF=-\frac{RV_Z}{D_Z}$ for the value of the impurity density gradient that give zero impurity flux, quantifies the balance of convective and diffusive impurity transport. Its derivation relies on the fact that the transport of a trace impurity species can be described locally by dividing the effective diffusivity ($D_{Z,eff}$) into a diffusive and a convective part. In the trace impurity limit, i.e., for $Zf_Z\to 0$ in Eq. (4), the impurity flux Γ_Z becomes a linear function of ∇n_Z, offset by a convective velocity or "pinch" V_Z. The resulting expression is

$$\Gamma_{n_Z}=-D_{Z,eff}\nabla n_Z=-D_Z\nabla n_Z+n_Z V_Z\iff \frac{R\Gamma}{n_Z}=D_Z\frac{R}{L_{n_Z}}+RV_Z, \quad (5)$$

where n_Z is the density of the impurity species and R is the major radius of the tokamak, and both the diffusion coefficient (D_Z) and the convective velocity (V_Z) are independent of ∇n_Z.[18] The right hand side of the equivalence is arrived at

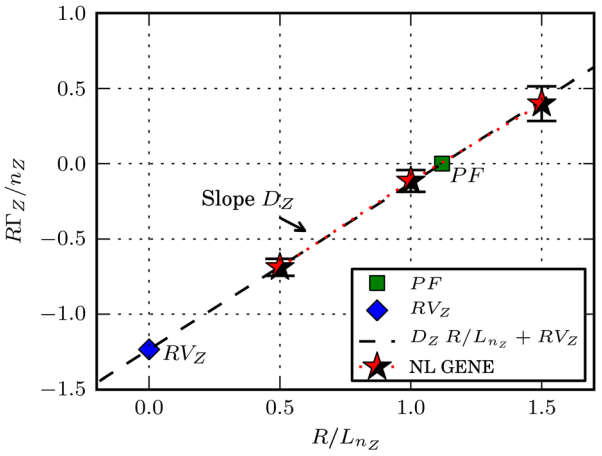

FIG. 1. Impurity flux (Γ_Z) dependence on the impurity density gradient ($-R\nabla n_Z/n_Z = R/L_{n_Z}$), illustrating the impurity PF, the diffusivity (D_Z), and pinch (RV_Z), and the validity of the linearity assumption in Eq. (5) of Γ_Z for trace impurities. Parameters of Eq. (5) are estimated from the calculated fluxes, taking the estimated error of the data into account. The flux is acquired as the average of a time series after convergence, as is illustrated in Fig. 3. Data from NL GENE simulations of TE mode driven turbulence with He impurities and parameters as in Fig. 4(a). The error bars indicate an estimated error of one standard deviation.

by assuming $-\nabla n_Z/n_Z = 1/L_{n_Z}$. The relationship of PF to D_Z and V_Z is illustrated in Fig. 1. Setting $\Gamma_Z = 0$ in Eq. (5) yields the interpretation of PF as the gradient of zero-impurity flux.

The impurity particle flux at the left hand side of Eq. (5) can be written as

$$\Gamma_{n_Z} = \langle \delta n_Z v_{E\times B}\rangle = -n_Z \rho_s c_s \left\langle \widetilde{n}_Z \frac{1}{r}\frac{\partial \widetilde{\phi}}{\partial \theta}\right\rangle. \tag{6}$$

The angled brackets imply a time and space average over all unstable modes. Performing this averaging for a fixed length scale $k_\theta \rho_s$ of the turbulence, the following expression is reached:

$$\begin{aligned}\frac{\Gamma_{n_Z}}{n_Z c_s} = \frac{k_\theta \rho_s \widetilde{\gamma}|\widetilde{\phi}_k|^2}{|N|^2}\Bigg\{ & \frac{R}{2L_{n_Z}}\left(|\widetilde{\omega}|^2 + \frac{14\tau_Z^*}{3}\widetilde{\omega}_r + \frac{55\tau_Z^{*2}}{9}\right) \\ & - \frac{R}{2L_{T_Z}}\left(2\tau_Z^*\widetilde{\omega}_r + \frac{10\tau_Z^{*2}}{3}\right) \\ & - \langle\lambda\rangle\left(|\widetilde{\omega}|^2 + \frac{10\tau_Z^*}{3}\widetilde{\omega}_r + \frac{35\tau_Z^{*2}}{9}\right) \\ & + \frac{Z}{3A_Z q_*^2 |N_1|^2}\Bigg[\tau_Z^*\left(\frac{19}{3}\widetilde{\omega}_r^2 - \frac{1}{3}\widetilde{\gamma}^2 + \frac{100\tau_Z^*}{3}\widetilde{\omega}_r - 5\tau_Z^{*2}\right) \\ & + 2\widetilde{\omega}_r|\widetilde{\omega}|^2\Bigg]\Bigg\},\end{aligned} \tag{7}$$

where $N_1 = \widetilde{\omega} - 2\tau_Z^*$ is introduced.

In the fluid model, it is assumed that the turbulence is isotropic in the radial and poloidal directions (r and θ, respectively; $k_r\rho_s = k_\theta\rho_s$), with a saturated fluctuation level estimate, based on nonlinear fluid simulations, of $|\phi_k| = \frac{\gamma}{\omega_{*e}}\frac{1}{k_\theta L_{n_e}}$.[34] A brief review of the different mechanisms responsible for the impurity transport, as identified in previous studies,[5,10,18] is given here. The first term in Eq. (7) corresponds to the diffusive part of Eq. (5), whereas the three subsequent terms correspond to the convective part of the transport of the impurity species. Of this, the R/L_{T_Z} term is the thermodiffusion, the sign of which is governed mainly by the real frequency, $\widetilde{\omega}_r$. For TE modes, $\widetilde{\omega}_r > 0$, and for ITG modes, $\widetilde{\omega}_r < 0$, resulting the thermodiffusion generally giving an inward pinch for TE modes and an outward pinch for ITG modes. Due to the Z-dependence in τ_Z^*, this term scales as $V_Z^{\nabla T} \sim (1/Z)(R/L_{T_Z})$ to leading order, rendering it unimportant for large Z impurity species, but it is important for lighter elements, such as the Helium ash. Further, the $\langle\lambda\rangle$ term gives the curvature pinch, which is usually inward, and the final term is the parallel compression term for the impurities. As opposed to the thermodiffusion, the parallel compression pinch is usually outward for TE modes and inward for ITG modes. Its Z dependence is $V_Z^{\parallel} \sim Z/A_Z k_\parallel^2 \sim Z/A_Z q^2$, but since $A_Z \approx 2Z$, this is expected to be a very weak scaling.[18] Effects of toroidal rotation on the impurity transport have recently been studied,[11,30] but will not be considered here.

B. Gyrokinetics—The GENE code

The GENE code[37] is a massively parallel gyrokinetic Vlasov code, solving the nonlinear time evolution of the gyrokinetic distribution functions on a fixed grid in phase space.[31–33] The gyrokinetic equations are derived from the kinetic equations by performing an average of the particle gyrations around the field lines, so that the equations follow the centre of gyration, rather than the explicit orbits.[38–41] This reduces the velocity space coordinates from three to two directions: parallel and perpendicular velocity. Following the conventions of GENE, these are referred to as v and μ, respectively. In real space, the radial (x) and bi-normal (y) dependencies are treated spectrally, i.e., those directions are discretised explicitly in k-space, whereas the toroidal (z) direction is discretised in real space.

In this paper, GENE simulations are performed in a flux tube geometry with periodic boundary conditions in the perpendicular directions.[42,43] Its application relies on the assumption that the scales of the phenomena of interest are all small compared to the length scales associated with the driving gradients. This is usually fulfilled in the core of the plasma. A cross-section of the flux tube is presented in Fig. 2. There the size of the turbulent features can be seen, and a comparison of their size to the flux tube's perpendicular resolution of $\sim 125 \times 125$ main ion gyro-radii and the overall box size indicates that the resolution and flux tube dimensions are adequate; see Sec. III for more details on how the resolution was chosen.

The data presented in Fig. 2 are computed from the raw field data. By integrating further, scalar quantities can be obtained, quantities that are useful in comparing both with theoretical, experimental, and other numerical results. In this study, the scalar impurity flux Γ_Z is of most interest. Time series showing the fluctuations in the main ion density and the impurity flux for a nonlinear GENE simulation are presented in Fig. 3.

GENE can also be run in quasilinear mode, a method that is considerably less demanding when it comes to

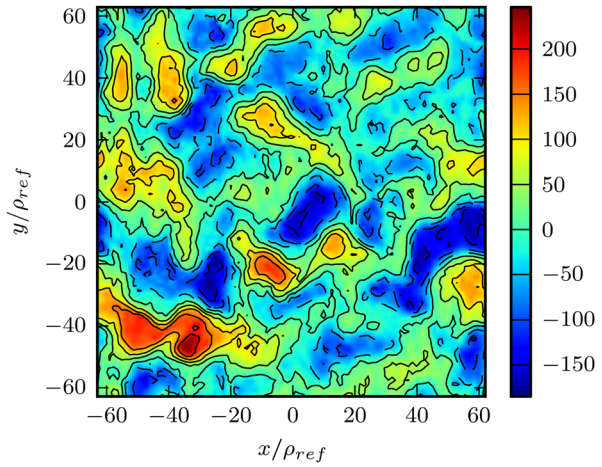

FIG. 2. A cross-section of the flux tube, showing the fluctuation of the electrostatic potential ϕ. Data from NL GENE simulation of TE mode turbulence, with parameters as in Fig. 4(a) at $t \approx 300R/c_s$.

computer resources.[32,33,44] The method used here only captures the contribution from the most unstable mode, ignoring sub-dominant modes, and only for the particular poloidal length scale $k_\theta \rho_s$ of choice. If the length scale is chosen appropriately, however, the quasilinear simulations are useful for getting a qualitative understanding of the physical processes. The QL model used here does not include a saturation condition to determine the absolute flux. In the QL results presented below, the peaking factor is obtained as a ratio between two fluxes and is hence independent of the fluctuation level. A more extensive quasilinear kinetic study, accounting for all unstable modes and summing over a wave number spectrum, was presented in Ref. 9.

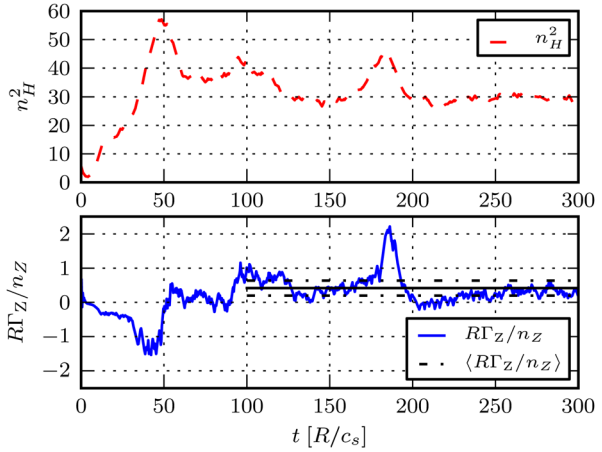

FIG. 3. Time series showing fluctuations in the main ion density (n_H^2) and impurity flux (Γ_z) after averaging over the whole flux tube (see Fig. 2). The averaged impurity flux ($\langle\Gamma_Z\rangle$) is calculated from Γ_Z, discarding the first portion to ensure that the linear phase of the simulation is not included. $\langle\Gamma_Z\rangle$ is used for finding the peaking factor for the impurity species, as is illustrated in Fig. 1. The bursty nature of the transport is seen in the peak around $t \approx 185R/c_s$. These bursts have been found to affect the average flux little but to significantly increase the estimated error in $\langle\Gamma_Z\rangle$ ($- \cdot -$). Data from NL GENE simulation of TE mode driven turbulence with He impurities. The parameters are the same as in Fig. 4(a), with $-R\nabla n_Z/n_Z = R/L_{n_Z} = 1.5$.

III. SIMULATIONS

In this paper, the transport of impurities has been studied numerically, by calculating the impurity *PF* for impurities with various impurity charge (Z) and varying values of the driving background gradients. The process of calculating the peaking factor is illustrated in Fig. 1. The impurity particle flux Γ_Z is computed for ∇n_Z in the vicinity of $\Gamma_Z = 0$, taking the estimated residuals of the samples' uncertainties into account (see Fig. 3). The diffusivity D_Z and convective velocity RV_Z are then given by fitting the acquired fluxes to Eq. (5), whereafter the peaking factor is obtained as $PF = -\frac{RV_Z}{D_Z}$ (see Sec. II A).

The instabilities causing the transport are fuelled by the free energy present in gradients in the system, and in general, the steeper the gradient the more free energy is available, which is expected to lead to stronger modes and more pronounced transport. Two families of gradients are available that can drive the instabilities: the temperature gradients ($-R\nabla T_j/T_j \approx R/L_{T_j}$) and the density gradients ($-R\nabla n_j/n_j \approx R/L_{n_j}$), where $j = i, e$ for main ions and electrons, respectively.[45] Numerical studies have been performed, focused on the dependence of the peaking factor on these gradients.

The main parameters used in the simulations are summarised in Table I. The parameters were chosen to represent an arbitrary tokamak geometry at about mid radius and do not represent any one particular experiment. As can be seen in the table, a TE or an ITG mode dominated plasma was studied by choosing a steep electron temperature gradient ($R/L_T = 7.0$) together with a moderate ion temperature gradient ($R/L_{T_i} = 3.0$) to prompt TE mode dominated dynamics and the other way around for ITG mode dominance. It should be noted in this context that TE modes can also be driven by steep density gradients. This case is omitted here and left for future study. In order to preserve quasineutrality, Eq. (4), $\nabla n_e = \nabla n_i$ was used. The simulations are limited to cases with $T_e = T_i$.

In order to ensure that the resolution was sufficient, the resolution was varied separately for the perpendicular, parallel, and velocity space coordinates, and the effects of this on the mode structure, $k_\perp$ spectra, and flux levels were investigated. The resolution was then set sufficiently high for the effects on these indicators to have converged. For a typical NL simulation

TABLE I. Parameters used in the gyrokinetic simulations.

	ITG	TE
T_i/T_e	1.0	1.0
s	0.8	0.8
q	1.4	1.4
$\epsilon = r/R$	0.14	0.14
$k_\theta \rho_s$	0.2	0.2
$n_e, n_i + Zn_Z$	1.0	1.0
n_Z *(trace)*	10^{-6}	10^{-6}
$R/L_{n_{i,e}}$ [a]	2.0–3.0	2.0–3.0
$R/L_{T_i}, R/L_{T_Z}$ [a]	7.0	3.0
R/L_{T_e} [a]	3.0	7.0

[a]Scan parameter.

for main ions, fully kinetic electrons, and one trace species, a resolution of $n_x \times n_y \times n_z = 96 \times 96 \times 24$ grid points in real space and of $n_v \times n_\mu = 48 \times 12$ in velocity space was chosen. For QL GENE simulations, the box size was set to $n_x \times n_y \times n_z = 8 \times 1 \times 24$ and $n_v \times n_\mu = 64 \times 12$, respectively.

Simulations have been performed with both deuterons and protons as main ions, but no significant differences in the impurity transport were found between the two cases.

The impurities were included self-consistently as a third species in the simulations, with the trace impurity particle density $n_Z/n_e = 10^{-6}$ in order to ensure that they have a negligible effect on the turbulence.

In the present study, a simple s–α geometry is assumed for the simulation domains. The effects of different tokamak geometries on drift wave turbulence have been studied in both fluid[46,47] and gyrokinetic descriptions.[48,49]

IV. RESULTS AND DISCUSSION

For the scalings studied, the charge number Z of the impurities was varied from $Z=2$ to $Z=74$ with a mass to charge ratio $A/Z=2$. The scalings of the peaking factor with the temperature gradients were studied by varying R/L_{T_e} between $R/L_{T_e} = 6.0$ and $R/L_{T_e} = 10.0$ for the TE mode case and similarly by varying $R/L_{T_{i,Z}}$ between $R/L_{T_{i,Z}} = 6.0$ and $R/L_{T_{i,Z}} = 10.0$ for the ITG mode case. The density gradient scalings were obtained by varying R/L_{n_e} between $R/L_{n_e} = 0.5$ and $R/L_{n_e} = 5.0$.

QL and NL scalings of $PF = -RV_Z/D_Z$ were obtained using GENE and compared to results obtained from the fluid model.

A. Scalings with impurity charge

The Z scalings of the impurity peaking factor for the TE mode dominated case are presented in Fig. 4(a). A good agreement between fluid and NL gyrokinetic results is observed for the value $k_\theta \rho_s = 0.2$ used in the QL and fluid simulations. The peaking factors are larger and the trends are more pronounced in the QL GENE results, which overestimate the peaking factors by approximately a factor of two for low Z impurities. As expected from the discussion in Sec. II, PF varies the most for low Z impurities where the thermopinch is stronger. For heavier elements, the peaking factor saturates at levels well below neoclassical predictions, as seen in previous gyrokinetic and fluid studies, of both TE and ITG mode dominated impurity transport.[17–19,21–23,30]

For comparison, the results for the ITG mode dominated case is shown in Fig. 4(b). The two cases show a qualitative difference, with PF falling towards saturation as Z is increased for the TE mode case, while the opposite holds for the ITG mode case. This is in line with previous QL kinetic and fluid results.[17–19,22,23] The peaking factor is close to zero for low Z values in the ITG mode dominated case; however, the sign of PF remains positive for all Z in both the TE and the ITG mode dominated case considered. This indicates that a net inward pinch is the most common situation in both *TE* and *ITG* mode driven impurity transport, for the parameters considered. It is, however, known from QL as well as NL gyrokinetic simulations that the convection of the impurities

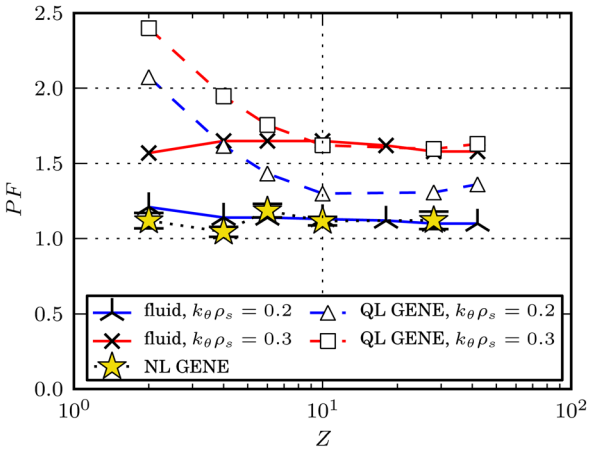

(a): dependence of the impurity peaking factor (PF) on Z for the TE case

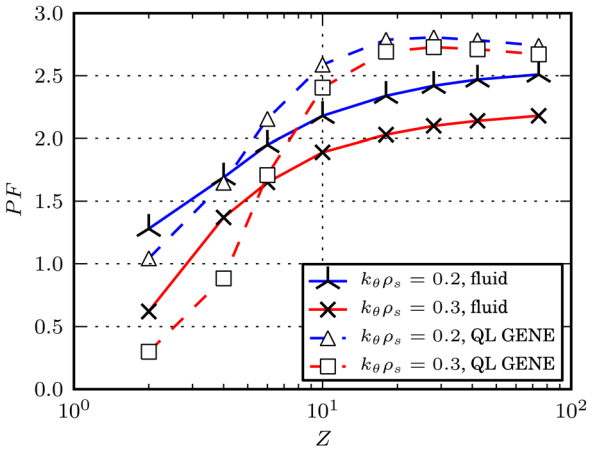

(b): dependence of the impurity peaking factor (PF) on Z for the ITG case

FIG. 4. Scalings of the impurity PF with impurity charge (Z). Parameters are $q=1.4$, $s=0.8$, $\epsilon = r/R = 0.143$ in both subfigures, with $R/L_{T_i} = R/L_{T_Z} = 3.0, R/L_{T_e} = 7.0, R/L_{n_e} = 2.0$ for the TE case (a), and $R/L_{T_i} = R/L_{T_Z} = 7.0, R/L_{T_e} = 3.0, R/L_{n_e} = 3.0$ for the ITG case (b). The error bars for the NL GENE results in (a), which indicate an estimated error of one standard deviation.

can reverse its direction, if the electron heat flux significantly exceeds the ion heat flux.[18,21]

The qualitative difference between the Z scalings for the TE and ITG mode dominated cases can be understood from the balance of the thermodiffusion and parallel impurity compression in Eq. (7), the two terms having opposite signs for TE and ITG, as discussed in Sec. II A. The parallel impurity compression is almost independent of Z, so it can be assumed that the thermodiffusion is the main contributor to the observed trends. The thermodiffusion, on the other hand, has the strongest effect for low Z values, explaining the drop and rise of PF with Z for the TE and ITG modes, respectively. Since this term goes to zero for large values of Z, this also explains the observed saturation.

Next, we compare the transport of He in TE and ITG mode driven turbulence. For efficient removal of the helium ash, the ratio between the energy confinement time and the He ash removal time should fulfil $\tau_E/\tau_{He} \geq 0.15$.[50] This confinement time ratio is usually estimated by the $D_{He,eff}/\chi_{eff}$ ratio. Assuming $T_e = T_i$, the effective heat conductivity of the plasma can be defined as

$$\chi_{eff} = \frac{\chi_e R/L_{T_e} + \chi_i R/L_{T_i}}{R/L_{T_e} + R/L_{T_i}}. \quad (8)$$

We note from Eq. (5) that the convective fluxes will reduce $D_{He,eff}$ to a similar degree for the TE and ITG mode dominated cases since the helium peaking factors ($PF_{He} = -RV_{He}/D_{He}$) are nearly identical, with $PF_{He} \approx 1.2$ for both the NL GENE and fluid model in the TE case and $PF_{He} \approx 1.3$ for the fluid model in the ITG mode dominated case. The latter is also very near to the NL GENE and fluid peaking factors for helium seen in a previous study.[23] For a simple comparison between the two cases, it is, therefore, sufficient to compare the ratios D_{He}/χ_{eff}. For the TE mode dominated case, we find $D_{He}/\chi_{eff} = 1.7$ and 1.3 using the fluid model and NL GENE, respectively. For the ITG case, the fluid model yields $D_{He}/\chi_{eff} = 1.1$, which is comparable to the ratio 1.0 acquired using NL GENE in a previous study of ITG mode driven impurity transport.[23] The results indicate that TE mode turbulence is at least as efficient as ITG turbulence at removing He ash for the parameters studied.

In the fluid treatment, a strong ballooning eigenfunction is assumed with $k^2_{\|,sb} = (3q^2R^2)^{-1}$.[36] Since the contribution from the parallel compression pinch depends on the mode structure along the field line, the results are expected to be sensitive to the choice of $k_\|$. To investigate the sensitivity of the fluid results to the mode structure, a simplified treatment was used, varying $k_\|$ around its strong ballooning value while keeping the eigenvalues fixed. The results are shown in Fig. 5 for $k_\theta\rho_s = 0.2$ and 0.3 in the TE and ITG mode dominated cases. As observed, the peaking factors for TE mode turbulence is sensitive to the choice of $k_\|$, with the peaking factor going from $PF \approx 2$ to $PF \approx 0$ when $k^2_\|$ is varied from 0.5 to 2 times its strong ballooning value.

As is evident from Fig. 4, the value of PF is also dependent on the choice of $k_\theta\rho_s$, the perpendicular length scale. Finding the $k_\theta\rho_s$ that allows the QL gyrokinetic and fluid models to best capture the behaviour of the impurity transport is non-trivial. For the cases considered, the results were obtained with $k_\theta\rho_s = 0.2$. This is in line with previous results regarding comparisons of fluid and NL gyrokinetic results.[20] The nonlinear spectra for the fluctuations in the background electrostatic potential (ϕ) are illustrated in Fig. 6 for the TE and ITG mode dominated cases in Fig. 4.

The spectra both show a peak in the fluctuations at $k_\theta\rho_s \approx 0.15$, well below the wave number of maximum linear growth rate, $k_\theta\rho_s \approx 0.3$. We have confirmed that for $k_\theta\rho_s$ in the range 0.15–0.4, qualitatively similar QL results are obtained. In the following, $k_\theta\rho_s = 0.2 - 0.3$ will be used.

A further complication that arises when studying TE mode turbulence is the onset of electron temperature gradient (ETG) driven modes. For the parameters considered, these are mostly sub-dominant, and so are not captured by the QL treatment, but may give a nonlinear contribution through the nonlinear coupling between the small scale ETG modes and the longer wave lengths of the dominant TE modes, and care has to be taken to avoid this effect.[51,52]

B. Scalings with the temperature gradients

The obtained scalings of PF with the electron temperature gradient are presented in Fig. 7(a). We note that the QL gyrokinetic simulations overestimate the peaking factors by up to ~50%. The fluid results are in good agreement with the NL GENE results. Only weak trends were observed, in compliance with previous studies.[20,22,35] As with the Z scaling in Fig. 4(a), the NL trend is less pronounced, reaching saturation for lower values of R/L_{T_e} than the other two models.

For comparison, the results for the ITG mode dominated case are shown in Fig. 7(b). As was observed for the Z scaling in Sec. IV A, the trends for the TE and ITG mode

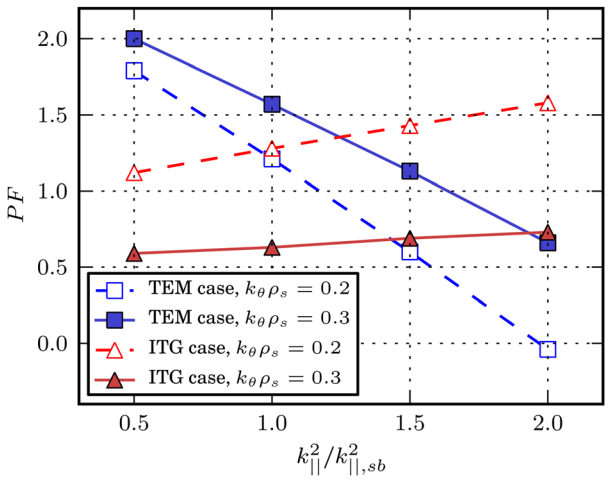

FIG. 5. Scaling of the impurity PF with $k^2_\|/k^2_{\|,sb}$ for He impurity, where $k^2_{\|,sb} = (3q^2R^2)^{-1}$ is the strong ballooning value;[36] fluid results with parameters as in Fig. 4(a) (TE) and Fig. 4(b) (ITG).

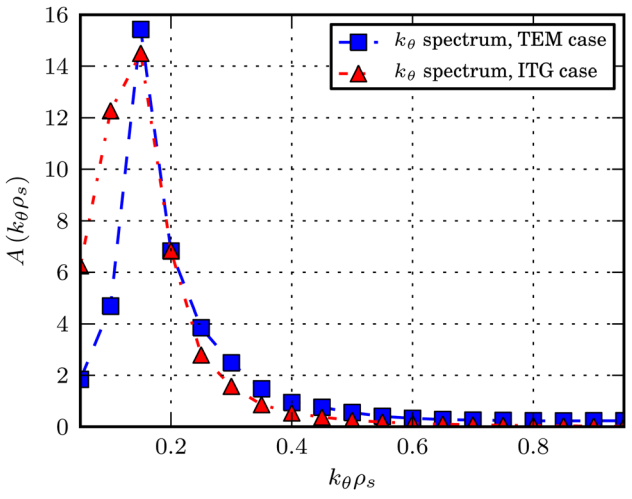

FIG. 6. Spectra showing the normalised amplitude ($A(k_\theta\rho_s)$) of the fluctuations in the background electrostatic potential (φ) as a function of $k_\theta\rho_s$; NL GENE results with parameters as in Fig. 4(a) (TE) and Fig. 4(b) (ITG).

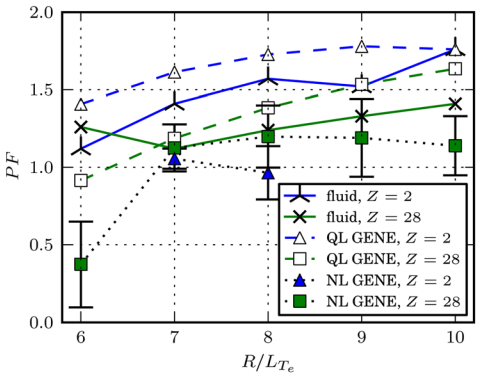

(a): dependence of the impurity peaking factor (PF) on the normalised electron temperature gradient for the TE case

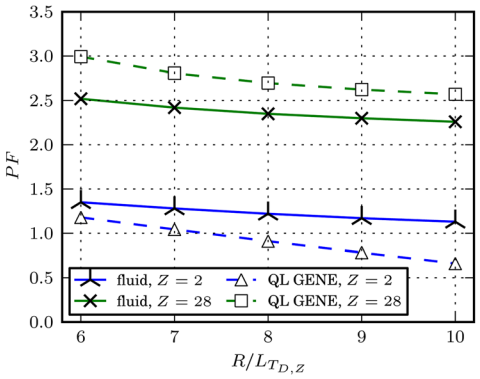

(b): dependence of the impurity peaking factor (PF) on the normalised ion temperature gradient for the ITG case;

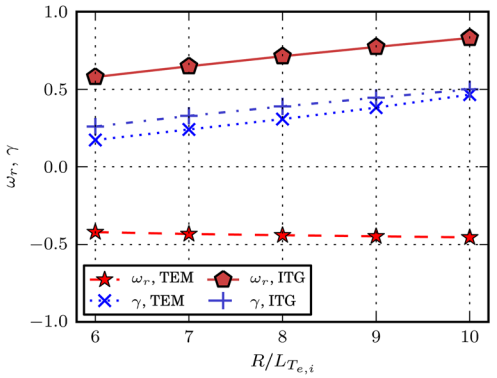

(c): real frequency (ω_r) and growth rate (γ) for the two cases in (a) and (b)

FIG. 7. Scalings of the impurity PF with the electron and ion temperature gradients ($-R\nabla T_{e,i}/T_{e,i} = R/L_{T_{e,i}}$). Parameters for the TE and ITG mode case as in Fig. 4, with $k_\theta \rho_s = 0.2$. The eigenvalues in (c) are from QL GENE simulations; they are normalised to c_s/R.

dominated case are reversed; PF rises with driving gradient for the TE case but falls for the ITG case. The difference between the two trends can be understood in part from the thermodiffusion in Eq. (7). This term grows more important as the ion/impurity temperature gradient steepens, providing a strong outward pinch for the ITG mode dominated impurity transport and thus yielding lower values of PF as R/L_{T_Z} increases (Fig. 7(b)). Since the impurity temperature gradient is constant for the ∇T_e scaling, however, other effects are behind the TE mode scaling in Fig. 7(a). The eigenvalues, in particular the mode growth rates, grow with $\nabla T_{e,i}$, as shown in Fig. 7(c). This will alter the relative contributions of the convective terms in Eq. (7) and hence affect the peaking factor. We note here that the eigenvalues in Fig. 7(c) are normalised to c_s/R, giving $\omega_r < 0$ for TE modes and $\omega_r > 0$ for ITG modes.

As with the Z scaling, the sign of PF usually remains positive for the $\nabla T_{e,i}$ scalings, though a modest flux reversal is observed when the trends of the scalings with Z and R/L_{T_i} for the ITG mode combine. This is the case for He in Fig. 7(b). The flux reversal is observed only for very steep temperature gradients for the considered parameter values with $T_e = T_i$.

C. Scalings with density gradient

In experimentally relevant situations where the impurity and main ion fuelling originates from the edge, the core impurity and background density peaking factors should be calculated self-consistently for zero particle flux. For this purpose, the equations $\Gamma_Z = 0$ and $\Gamma_{i,e} = 0$ need to be solved self-consistently. This is, in the following, achieved by varying the main ion density gradient R/L_{n_e} until $\Gamma_e = 0$ is obtained and using the zero flux background density gradient in the impurity transport calculations. We assume trace levels of impurities and use the fluid model for simplicity. The results are illustrated in Fig. 8 which shows the impurity peaking factor R/L_{n_z} versus R/L_{n_e} for both the TE and ITG mode dominated cases. The value of R/L_{n_e} for zero background particle flux is marked in the figure. We note that the background density peaking is larger than the impurity peaking with $R/L_{n_e} \approx 2.5$ for both the TE and the cases. We emphasise that the result is obtained using a collision-less model. It is known that collisions have a large impact on the background density peaking in both fluid[23] and gyrokinetic models.[53]

For the R/L_{n_e} scaling, the same trends are observed in both QL GENE and fluid data, with a strong sensitivity for lower Z impurities. This is particularly evident for the ITG mode case in Fig. 8(b), where the peaking factor for the He impurity shows a marked increase as ∇n_e steepens for both GENE and fluid results, whereas for the heavier elements, a nearly flat dependence is observed.

As shown in Fig. 8(c), the eigenvalues vary with the electron density gradient. A reduction of $|\omega_r|$ and an increase of γ are observed with increasing R/L_{n_e}, which leads to a reduction of the relative amplitude of the thermopinch in Eq. (7). This explains the observed PF scaling for the TE and ITG mode driven cases in Figs. 8(a) and 8(b), respectively.

As with the ∇T_i scaling, the combined effect of the Z and ∇n_e scalings is observed to lead to a flux reversal for the He impurity in the ITG mode dominated case in Fig. 8(b). This happens for flat electron density profiles in

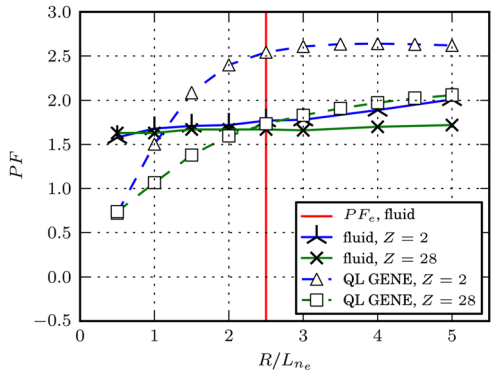

(a): dependence of the impurity peaking factor (PF) on the normalised electron density gradient for the TE case, also indicated is the main ion peaking factor (PF_e) from fluid theory

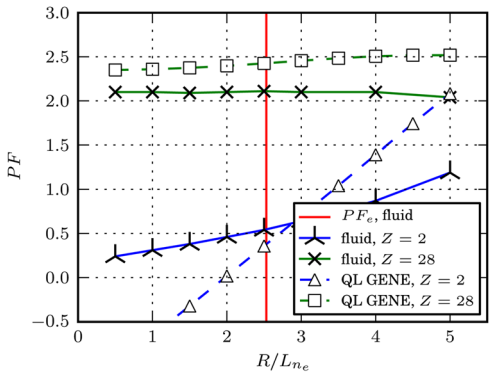

(b): dependence of the impurity peaking factor (PF) on the normalised electron density gradient for the ITG case, also indicated is the main ion peaking factor (PF_e) from fluid theory

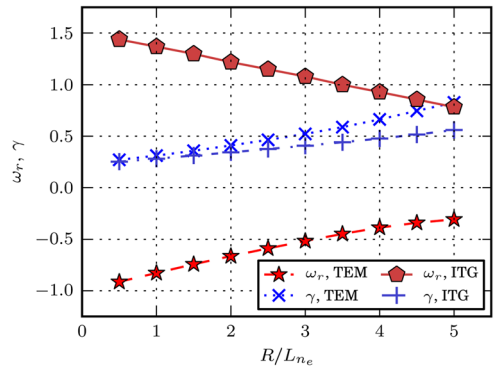

(c): real frequency (ω_r) and growth rate (γ) for the two cases in (a) and (b)

FIG. 8. (Color online) Scalings of the impurity PF with the electron density gradient ($-R\nabla n_e/n_e = R/L_{n_e}$); also indicated is the main ion peaking factor (PF_e) from fluid theory. Parameters for the TE and ITG mode cases as in Fig. 4, with $k_\theta \rho_s = 0.3$ for both cases. The eigenvalues in (c) are from QL GENE simulations; they are normalised to c_s/R.

the QL GENE results. Outside of this regime the sign of PF remains positive.

V. CONCLUSION AND FUTURE WORK

In the present paper, the transport of impurities driven by TE mode driven turbulence has been studied. NL gyrokinetic simulations using the code GENE were compared with results from QL gyrokinetic simulations and a computationally efficient fluid model, viable for use in predictive simulations. The main focus has been on model comparisons for electron temperature gradient driven turbulence regarding the sign of the main ion and impurity convective velocities (pinches) and the peaking factors (R/L_{n_j}) for zero particle flux. In particular, the scaling of the impurity peaking factor with impurity charge Z and with driving temperature gradient has been investigated and compared with the more well known results for ITG driven turbulence. In addition, the removal of helium ash in TE/ITG mode turbulence has been investigated.

For the scaling of the impurity peaking factor with the impurity charge Z, a weak dependence was obtained from NL GENE simulations, which was reproduced well by the fluid simulations. The QL GENE results showed a stronger dependence for low Z impurities and overestimated the peaking factor by up to a factor of two in this region. As in the case of ITG dominated turbulence, the peaking factors were found to saturate as Z increased, at a level much below neoclassical predictions. However, the scaling with Z was found to be weak or reversed as compared to the ITG case, where the larger peaking factors were obtained for high Z impurities.

The He ash removal was studied through a comparison of the ratio of the particle diffusivity and effective heat conductivity (D_{He}/χ_{eff}), using both NL GENE and fluid simulations. The obtained results indicated that TE mode turbulence is at least as efficient as ITG turbulence at removing He ash for the parameters studied, with $D_{He}/\chi_{eff} > 1.0$ for both modes of turbulence. A comprehensive investigation, however, would require a predictive global transport simulation with multiple species, including He sources, which is beyond the scope of the present work.

The scaling of impurity peaking with the driving background temperature gradients was found to be weak in most cases. The QL results were also here found to significantly overestimate the peaking factor for low Z values.

The main ion peaking relative to the impurity peaking was studied using a self-consistent treatment of the main ion and impurity particle fluxes. It was found that the main ion peaking was slightly larger than the impurity peaking, for both TE and ITG mode dominated turbulence. These results were obtained using the fluid model in the collision-less limit.

The fluid and QL GENE results were shown to be sensitive to the choice of poloidal wave number. For the parameters studied, the best agreement with the results from the NL GENE simulations was obtained for $k_\theta \rho_s = 0.2$. Better agreement may be obtained by employing an extended QL model, accounting for all unstable modes and summing over

a wave number spectrum. In general, however, only a nonlinear simulation can determine the spectrum that best approximates the transport features for a given set of parameters. Using the fluid model it was further shown that the impurity peaking factors in the TE mode dominated case are sensitive to the mode structure along the field lines ($k_\parallel$) through the parallel compression pinch. Assuming a strong ballooning eigenfunction with $k_\parallel^2 = (3q^2R^2)^{-1}$ gave a good agreement with the results from the NL GENE simulations.

The present study is based on low β plasmas in a simple s–α circular tokamak equilibrium. Future work will aim to study the effects of more realistic geometries, finite β, as well as effects of plasma rotation on impurity transport in NL fluid and gyrokinetic descriptions.

ACKNOWLEDGMENTS

The simulations were performed on resources provided on the Lindgren[54] and HPC-FF (Ref. 55) high performance computers, by the Swedish National Infrastructure for Computing (SNIC) at Paralleldatorcentrum (PDC) and the European Fusion Development Agreement (EFDA), respectively. J. Vincent at PDC and T. Görler at IPP–Garching are acknowledged for their assistance concerning technical and implementational aspects in making the GENE code run on the PDC Lindgren super-computer. A. Strand and L. Strand at Herrgårdsskolan are acknowledged for their help with the nonlinear simulations. The authors would also like to thank F. Jenko, M. J. Püschel, F. Merz, and the rest of the GENE team at IPP–Garching for their valuable support and input.

[1]C. S. Harte, C. Suzuki, T. Kato, H. A. Sakaue, D. Kato, N. Tamura, S. Sudo, R. D'Arcy, E. Sokell, J. White, and G. O'Sullivan, J. Phys. B **43**, 205004 (2010).
[2]Also commonly referred to as the η_i mode.
[3]M. Fröjdh, M. Liljeström, and H. Nordman, Nucl. Fusion **32**, 419 (1992).
[4]R. Basu, T. Jessen, V. Naulin, and J. J. Rasmussen, Phys. Plasmas **10**, 2696 (2003).
[5]C. Estrada-Mila, J. Candy, and R. Waltz, Phys. Plasmas **12**, 022305 (2005).
[6]V. Naulin, Phys. Rev. E **71**, 015402 (2005).
[7]M. Priego, O. E. Garcia, V. Naulin, and J. J. Rasmussen, Phys. Plasmas **12**, 062312 (2005).
[8]T. Fülöp and J. Weiland, Phys. Plasmas **13**, 112504 (2006).
[9]C. Bourdelle, X. Garbet, F. Imbeaux, A. Casati, N. Dubuit, R. Guirlet, and T. Parisot, Phys. Plasmas **14**, 112501 (2007).
[10]N. Dubuit, X. Garbet, T. Parisot, R. Guirlet, and C. Bourdelle, Phys. Plasmas **14**, 042301 (2007).
[11]Y. Camenen, A. G. Peeters, C. Angioni, F. J. Casson, W. A. Hornsby, A. P. Snodin, and D. Strintzi, Phys. Plasmas **16**, 012503 (2009).
[12]T. Fülöp, S. Braun, and I. Pusztai, Phys. Plasmas **17**, 062501 (2010).
[13]S. Futatani, X. Garbet, S. Benkadda, and N. Dubuit, Phys. Rev. Lett. **104**, 015003 (2010).
[14]T. Hein and C. Angioni, Phys. Plasmas **17**, 012307 (2010).
[15]S. Moradi, M. Z. Tokar, and B. Weyssow, Phys. Plasmas **17**, 012101 (2010).
[16]T. Fülöp and S. Moradi, Phys. Plasmas **18**, 030703 (2011).
[17]H. Nordman, R. Singh, T. Fülöp, L.-G. Eriksson, R. Dumont, J. Andersson, P. Kaw, P. Strand, M. Tokar, and J. Weiland, Phys. Plasmas **15**, 042316 (2008).
[18]C. Angioni and A. G. Peeters, Phys. Rev. Lett. **96**, 095003 (2006).
[19]C. Angioni, L. Carraro, T. Dannert, N. Dubuit, R. Dux, C. Fuchs, X. Garbet, L. Garzotti, C. Giroud, R. Guirlet, F. Jenko, O. J. W. F. Kardaun, L. Lauro-Taroni, P. Mantica, M. Maslov, V. Naulin, R. Neu, A. G. Peeters, G. Pereverzev, M. E. Puiatti, T. Pütterich, J. Stober, M. Valovič, M. Valisa, H. Weisen, A. Zablotsky, ASDEX Upgrade team, and JET–EFDA contributors, Phys. Plasmas **14**, 055905 (2007).
[20]H. Nordman, T. Fülöp, J. Candy, P. Strand, and J. Weiland, Phys. Plasmas **14**, 052303 (2007).
[21]C. Angioni, A. G. Peeters, G. V. Pereverzev, A. Bottino, J. Candy, R. Dux, E. Fable, T. Hein, and R. E. Waltz, Nucl. Fusion **49**, 055013 (2009).
[22]T. Fülöp and H. Nordman, Phys. Plasmas **16**, 032306 (2009).
[23]H. Nordman, A. Skyman, P. Strand, C. Giroud, F. Jenko, F. Merz, V. Naulin, T. Tala, and the JET–EFDA contributors, Plasma Phys. Controlled Fusion **53**, 105005 (2011).
[24]R. Dux, R. Neu, A. G. Peeters, G. Pereverzev, A. Mck, F. Ryter, and J. Stober, Plasma Phys. Controlled Fusion **45**, 1815 (2003).
[25]M. E. Puiatti, M. Valisa, M. Mattioli, T. Bolzonella, A. Bortolon, I. Coffey, R. Dux, M. von Hellermann, P. Monier-Garbet, M. F. F. Nave, J. Ongena, and contributors to the EFDA–JET work programme, Plasma Phys. Controlled Fusion **45**, 2011 (2003).
[26]M. E. Puiatti, M. Valisa, C. Angioni, L. Garzotti, M. Mattioli, L. Carraro, I. Coffey, and C. Sozzi, Phys. Plasmas **13**, 042501 (2006).
[27]C. Giroud, R. Barnsley, P. Buratti, I. H. Coffey, M. von Hellermann, C. Jupén, K. D. Lawson, A. Meigs, M. O'Mullane, A. D. Whiteford, K.-D. Zastrow, and the JET–EFDA contributors, Nucl. Fusion **47**, 313 (2007).
[28]C. Giroud, C. Angioni, M. Barruzzo, M. Brix, G. Bonheure, P. Burratti, C. Challis, L. Carraro, I. H. Coffey, P. de Vries, J. Hobirk, E. Joffrin, X. Litaudon, J. Mailloux, M. O'Mullane, V. Naulin, H. Nordman, D. Strintzi, M. Valisa, A. D. Whiteford, K.-D. Zastrow, and JET–EFDA contributors, in 12th International Workshop on "H-mode Physics and Transport Barriers," Princeton, USA, 2009.
[29]P. Helander and D. J. Digmar, *Collisional Transport in Magnetized Plasmas* (Cambridge University Press, Cambridge, UK, 2002).
[30]C. Angioni, R. McDermott, E. Fable, R. Fischer, T. Ptterich, F. Ryter, G. Tardini, and the ASDEX Upgrade Team, Nucl. Fusion **51**, 023006 (2011).
[31]F. Jenko, W. Dorland, M. Kotschenreuther, and B. N. Rogers, Phys. Plasmas **7**, 1904 (2000).
[32]T. Dannert, "Gyrokinetische simulation von plasmaturbulenz mit gefangenen teilchen und elektromagnetischen effekten," Ph.D. dissertation, Technischen Universität München, 2005.
[33]F. Merz, "Gyrokinetic simulation of multimode plasma turbulence," Ph.D. dissertation, Westfälischen Wilhelms-Universität Münster, 2008.
[34]J. Weiland, *Collective Modes in Inhomogeneous Plasmas* (Institute of Physics Publishing (IoP), Bristol, UK, 2000).
[35]H. Nordman, P. Strand, and X. Garbet, J. Plasma Phys. **73**, 731 (2007).
[36]A. Hirose, L. Zhang, and E. Elia, Phys. Rev. Lett. **72**, 3993 (1994).
[37]See http://gene.rzg.mpg.de/ for details on GENE.
[38]T. M. Antonsen and B. Lane, Phys. Fluids **23**, 1205 (1980).
[39]E. A. Frieman and L. Chen, Phys. Fluids **25**, 502 (1982).
[40]T. S. Hahm, W. W. Lee, and A. Brizard, Phys. Fluids **31**, 1940 (1988).
[41]A. Brizard, J. Plasma Phys. **41**, 541 (1989).
[42]M. A. Beer, "Gyrofluid models of turbulent transport in tokamaks," Ph.D. dissertation, Princeton University, 1995.
[43]M. A. Beer, S. C. Cowley, and G. W. Hammett, Phys. Plasmas **2**, 2687 (1995).
[44]T. Dannert and F. Jenko, Phys. Plasmas **12**, 072309 (2005).
[45]The density and temperature gradients of the impurity species can also drive turbulent transport; however, for trace amounts this effect is negligible.
[46]J. Anderson, H. Nordman, and J. Weiland, Plasma Phys. Controlled Fusion **42**, 545 (2000).
[47]J. Anderson, T. Rafiq, M. Nadeem, and M. Persson, Phys. Plasmas **9**, 1629 (2002).
[48]D. Told and F. Jenko, Phys. Plasmas **17**, 042302 (2010).
[49]A. Bruckel, O. Sauter, C. Angioni, J. Candy, E. Fable, and X. Lapillonne, J. Phys.: Conf. Ser. **260**, 012006 (2010).
[50]D. Reiter, G. H. Wolf, and H. Kever, Nucl. Fusion **30**, 2141 (1990).
[51]D. R. Ernst, J. Lang, W. M. Nevins, M. Hoffman, and Y. Chen, Phys. Plasmas **16**, 055906 (2009).
[52]Z. Gao, H. Sanuki, K. Itoh, and J. Q. Dong, Phys. Plasmas **12**, 022503 (2005).
[53]C. Angioni, J. Candy, E. Fable, M. Maslov, A. G. Peeters, R. E. Waltz, and H. Weisen, Phys. Plasmas **16**, 060702 (2009).
[54]See http://www.pdc.kth.se/resources/computers/lindgren/ for details on Lindgren.
[55]See http://www2.fz-juelich.de/jsc/juropa/ for details on HPC-FF.